JOURNAL OF MATERIALS SCIENCE: MATERIALS IN MEDICINE 6 (1995) 94–104

Hydroxyapatite films on silicon single crystals by a solution technique: texture, supersaturation and pH dependence

P. E. WANG, T. K. CHAKI
Department of Mechanical and Aerospace Engineering, State University of New York, Buffalo, NY 14260-4400, USA

Thick films of hydroxyapatite (HA) were deposited on silicon single crystal wafers placed in close proximity to a plate of apatite- and wollastonite-containing glass and dipped into a simulated physiological solution at 36 °C. Amorphous calcium phosphate phase present in the glass leached into the solution, causing supersaturation of Ca^{2+} and PO_4^{3-} ions. Spherical cap-like islands of calcium phosphate nucleated on Si crystals and grew in size with time. The thickness of the film grown on Si (1 1 1) in a solution having a composition similar to that of human blood plasma, and maintained at pH of 7.2, reached 7.1 μm in 336 h, compared with a thickness of 12.7 μm when the ion concentrations of the solution were doubled. HA films grown on Si (1 1 1) showed strong (1 0 2) texture. In contrast, hardly any HA film could be grown on Si (1 0 0). With increasing pH value of the solution the Ca/P ratio of the film increased. At a pH of 7.2 the as-grown and annealed (at 800 °C for 3 h in argon) films had Ca/P ratios of 1.10 and 1.72, respectively. The Vickers hardness and the adhesion strength of the film increased upon annealing. Our results suggest that the driving force for formation of apatite films arises from the lowering of free energy of the supersaturated solution by deposition of ions (Ca, P, O, H) in certain crystallographic arrangements on suitable substrates with low interface energies.

1. Introduction

Hydroxyapatite (abbreviated as HA), being a major constituent [1] of bone, has good biocompatibility [2, 3]. Its chemical formula is $Ca_{10}(PO_4)_6(OH)_2$ and it crystallizes with a hexagonal structure [4] with unit cell dimensions $a = 0.9432$ nm and $c = 0.6881$ nm. HA powder can be formed [5] into blocks with various densities and strengths by pressureless sintering, hot pressing and hot isostatic pressing. The most interesting property of HA is that tissue and bone can bond [6] with HA. Studies of porous HA implants on dogs' alveolar ridges [7] and human maxillary alveolus [8] reported bone ingrowth into the open pores on the surface of the implants. In the case of dense HA implants, studies in dogs [9, 10] and biopsy specimens from humans [11, 12] showed that the implants became surrounded by mature fibrous tissue, with a variable amount of new bone formation. However, HA implants often developed cracks [10]. Load-bearing orthopaedic and dental implants must have adequate fracture toughness during use [13], in addition to being biocompatible. In fact, brittleness of HA is a serious obstacle to its use as load-bearing implants. Recently, Chaki and Wang [14] have shown that decomposition of HA hinders sintering at high temperatures and degrades mechanical properties of sintered HA compacts.

The coating of HA on metallic implants is receiving increasing attention. The coated implants will not only have the ductility of the underlying metal, but also have a biocompatible surface. There are a number of additional beneficial effects [15, 16] of the coating: faster adaptation of implant and surrounding tissue with reduced healing time [17], enhancement of bone formation [18], firmer implant–bone attachment [19, 20] and the reduction of metallic ion release [21]. HA coating has been applied to implants by various methods, such as electrophoretic deposition, sputtering, plasma spray, high velocity flame deposition and laser deposition. In electrophoretic deposition [18, 22] HA particles are precipitated on a substrate from a suspension of HA powder in isopropanol. The deposited coating is sintered above 900 °C to harden the coating. If the substrate is metallic, the sintering has to be done in vacuum to prevent oxidation. In the ion sputtering process [23, 24] an ion beam sputters off atoms and molecules from a HA target to form a thin coating on the substrate material in vacuum. In the plasma spraying process [16, 25] HA powder is blown through a high temperature arc discharge. The molten HA particles hit the metallic substrate and form a coating. In the high-velocity flame-spraying technique [26] HA particles pass (at a speed of 2–3 mach) through the high-temperature zone of an oxy-fuel

0957–4530

flame and hit a substrate, producing an adherent HA film. Recently, Cotell *et al.* [27] prepared HA films on Ti-6Al-4V substrates by pulsed laser deposition technique, in which pulses (150 mJ per pulse) from a KrF excimer laser were focused on a HA pellet target and plumes of ions and molecules were deposited on the substrate at a distance of 4 cm from the pellet.

All of the deposition processes described above involve high-temperature processing steps, some in vacuum. Thus, there is a possibility of dehydroxylation and decomposition [14] of HA in the coating. For instance, the plasma-sprayed HA coating contains tri- and tetra-calcium phosphates, oxyhydroxyapatite and amorphous calcium phosphates [16, 28, 29]. Ellies *et al.* [30] claimed that degradation of HA in plasma-sprayed coating is severe if the starting powder is calcium-deficient, and reported only 5% degradation in the coating deposited from stoichiometric HA powder. The biological response of tissues to various calcium phosphates depends [31, 32] on the crystal structure and therefore it is important to avoid degradation of the HA coating. Dissolution and resorption [33] of certain phases present in the HA coating can cause problems to fixation of coated implants.

Deposition of HA coating from solutions, mimicking the biological process in our body, can obviate the problem of decomposition which occurs during high-temperature processing. Hench *et al.* [34] discovered that implants made of certain glasses called Bioglass^R in the Na_2O–CaO–SiO_2–P_2O_5 system can directly contact the surrounding bone, forming a tight chemical bond with it. When placed in a simulated physiological solution as well as in living tissue, Bioglasses^R form first a silica-rich layer and then an apatite layer [35]. Recently, Abe *et al.* [36] reported that a HA coating can be formed on almost any substrate (metals, ceramics and polymers), placed in proximity to a Bioglass^R plate and dipped into a simulated body fluid at 36 °C. Even though the exact mechanism of formation of HA films in solutions is not understood at present, several explanations have been put forward. Hench [37] proposed that alkaline pH at the surface of the glass due to dissolution of ions causes supersaturation which promotes precipitation of calcium phosphate. Andersson and coworkers [38, 39] proposed that initially a silica gel is formed on the Bioglass^R surface and that calcium phosphate complexes with the silica gel, forming apatite crystals. Kokubo [40] suggested that calcium and silicate ions dissolve from the glass and cooperatively help formation of an apatite layer with silicate ions providing nucleation sites. Li *et al.* [41] proposed that the dissolution of amorphous calcium phosphate from the glass creates a negatively charged surface which attracts Ca^{2+} ions to the glass. In order to improve our understanding of the formation of the HA coating, here we present the results of an extensive experimental study of the growth of HA films from a simulated physiological solution on Si single crystals, including the results of the effects of orientation of the substrate, supersaturation of the solution, pH of the solution and annealing of the film. Our results shed light on the mechanism of formation of HA films from solution.

2. Materials and methods

Plates of apatite- and wollastonite-containing glass ceramic (AW-glass) were prepared by sintering. The starting composition (wt %) was CaO 44.7, SiO_2 34.0, P_2O_5 16.2, MgO 4.6 and CaF_2 0.5. The initial composition of our AW-glass was same as that of the glass used by Abe *et al.* [36], but our preparation method (consequently the contents) was different. The mixture of powders of reagent grade chemicals of the above composition was ball-milled in a rotating jar and was cold-pressed under a stress of 265 MPa inside a steel die into thin plates of dimension 48 × 20 × 5 mm. The compacted plate was placed centrally on an alumina plate of dimension 50 × 25 × 0.7 mm and sintered in air at 1300 °C for 2 h. There was partial melting of the powder compact during sintering (the melting point of P_2O_5 was only 580 °C), but the shape of the plate of AW glass was retained. The sintered plate of AW glass was cooled in the furnace with the lid of the furnace partially opened. After the furnace was shut off, the temperature was decreased from 1300 to 1000 °C in 30 min, to 875 °C in 60 min, to 750 °C in 90 min and to 675 °C in 120 min. The AW-glass plate cooled at this rate did not exhibit any crack to the naked eye or under an optical microscope at low magnifications (up to 100 ×). Due to diffusion during sintering the glass plate became bonded with the Al_2O_3 plate and no attempt was made to separate them. The underlying Al_2O_3 plate provided an added advantage (besides providing mechanical strength) that in the physiological solution leaching of ions took place only from the top surface of the glass plate. Due to partial melting the surface of the glass plate was not smooth. The top surface of the glass plate was polished to 5 μm, first with emery paper and then with Al_2O_3 slurry.

An aqueous solution was prepared by dissolving reagent grade NaCl, $NaHCO_3$, KCl, $K_2HPO_4 \cdot 3H_2O$, $MgCl_2 \cdot 6H_2O$, $CaCl_2$ and Na_2SO_4 in distilled water with proportions that yielded ion concentrations shown in the second column of Table I. This solution was buffered at pH of 7.25 with 50 mM tris-(hydroxymethyl) aminomethane ($(CH_2OH)_3CNH_2$) and 45 mM hydrochloric acid (HCl). This solution provided a simulated body fluid (1SBF), as its cation

TABLE I Ion concentrations (mM) in simulated body fluid (1SBF) and human blood plasma

Ion	1SBF	Blood plasma
Na^+	142.0	142.0
K^+	5.0	5.0
Ca^{2+}	2.5	2.5
Mg^{2+}	1.5	1.5
Cl^-	147.8	103.0
HCO_3^-	4.2	27.0
HPO_4^{2-}	1.0	1.0
SO_4^{2-}	0.5	0.5

concentrations were the same (Table I) as those in human blood plasma [42]. To study the effect of ion concentrations on deposition of HA film, another solution (2SBF) was prepared with ion concentrations twice those shown in the second column of Table I. The pH (monitored by a pH-meter) of 2SBF was maintained at various values in the range 5.2–9.2 by adding various amounts of HCl. In each deposition experiment about 500 ml of the solution was kept in a bottle made of high-density polyethylene, with the lid closed to avoid evaporation of water. In all experiments the temperature of 1SBF and 2SBF was maintained at 36 °C (the physiological temperature of human body) by placing the bottle in a water bath.

The substrates used in the present study for depositing HA films were wafers of silicon single crystals with one surface of the wafer polished smooth and shiny. The 76 mm diameter wafers cut along (1 1 1) and (1 0 0) planes within $\pm 1°$ were purchased from Pure-Sil, Inc. Both p-type (B-doped, resistivity 0.0055–0.0063 ohm cm) and n-type (P-doped, resistivity 0.20 ± 0.04 ohm cm) wafers were used. Since the nature of doping did not make any difference in deposition characteristics, we do not make any distinction between p- and n-type Si wafers in the future discussion. Substrates of dimension $60 \times 30 \times 0.4$ mm were cut from the wafer using a diamond blade. Silicon substrates were cleaned by Ishizaka–Shiraki method [43], in which the substrates were boiled in NH_4OH solution and then dipped in 2.5% HF solution for 10–15 s. The substrate was then placed centrally on the top of the AW-glass plate with a gap of 0.7 mm maintained with the help of two alumina spacers of dimension $25 \times 2 \times 0.7$ mm. Each spacer was placed near the edge of the glass plate with the length of the spacer along the width of the glass plate. The central part (about 40 mm in length) of the glass plate was exposed to the solution, facing the shiny surface of the Si substrate. The couple containing the glass plate and the substrate with Al_2O_3 spacers in between them was tied by cotton thread and dipped into the simulated body fluid in the polyethylene bottle. To remove any air bubbles entrapped in the gap of the couple, the bottle containing the couple was vibrated in an ultrasonic bath for 10 min.

After a few days of immersion in the simulated body fluid the substrate was untied and examined visually and by light microscopy at a low magnification ($100\times$) to check if any film had grown. In every deposition experiment fresh solution and a new AW-glass plate were used. In many experiments the solution was replaced by a fresh one every 24 h. The thickness of the film was measured by a surface profilometer (Alpha-Step 200, made by Tencor Instruments), measuring up to 20 nm. The phases present in the film were determined by a Nicolet X-ray diffractometer with CuK_α radiation in transmission mode on apatite powder scraped from the substrate, as well as in the reflection mode on the films. Some of the films were annealed at 800 °C for 3 h in argon and examined again by X-ray diffraction. After dipping in the solution, some powder was scraped from the surface of the AW-glass plate to a depth of 0.25 mm and examined by X-ray diffraction. The diffraction patterns of the film and AW-glass were compared with the database in American Society for Testing and Materials powder diffraction files.

The Ca/P atomic ratio of the films grown at various pH values of the simulated body fluid was measured by chemical analysis. The film scraped from the substrate was dissolved in 50% concentrated HCl, and the concentration of Ca ions in the solution was measured by atomic absorption spectrometry. The concentration of PO_4 ions was determined from the ultraviolet absorption spectrum of a molybdivanadophosphate complex [44]. The microstructure of the AW-glass plate and the apatite films were examined using optical microscopy and scanning electron microscopy (SEM).

Hardness tests were performed on apatite films by Vickers indentation with loads in the range 10–100 g. The diagonal length of the impression due to indentation was plotted against the load. Beyond a certain load (called the critical load) the length of the impression increased rapidly owing to cracking of the film. Vickers hardness H_V of the as-grown and annealed films was determined at the critical load by using the formula:

$$H_V = \frac{2P\sin\alpha/2}{d^2} \quad (1)$$

where P is the applied load, d is the diagonal length of the impression and α is the apex angle of the pyramid-shaped indenter. α is 136° for the Vickers indenter.

The adhesion strength between the film and the substrate was measured by the scratch test [45] using a diamond indenter having a tip radius of about 30 μm. The scratch was made by moving the substrate manually at a speed of 0.025 mm s^{-1} under constant loads in the range 10–100 g. The width of the scratch was measured by optical microscopy and plotted against the load. The critical load at which the width increased rapidly due to decohesion of the film was noted. The adhesion strength (σ_{ad}) was calculated from the formula [46]:

$$\sigma_{ad} = \frac{2P}{\pi W\sqrt{R^2 - W^2/4}} \quad (2)$$

where P is the critical load, W is the width of the scratch and R is the radius of curvature of the tip of the indenter.

3. Results and discussion

3.1. Kinetics of growth

Upon immersion of the couple containing the AW-glass plate and Si substrate into 1SBF with a pH of 7.2 for more than a day, a white calcium phosphate film was seen (by the naked eye) to deposit on the Si (1 1 1) surface. Fig. 1 shows the surface profile of the film after deposition for 72 h. The surface of the film was uneven near the edge. The average thickness (as measured by the profilometer) of the middle part of the film was 1.5 ± 0.1 μm. In contrast, hardly any apatite film could be grown on the Si (1 0 0) surface. After immersion for

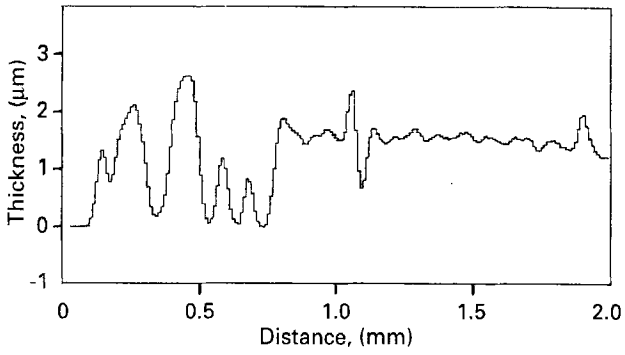

Figure 1 Surface profile of an apatite film grown on Si (1 1 1) in 1SBF solution (having cation concentrations same as those in human blood plasma) at pH of 7.2 for 72 h. The load on the stylus was 9 mg.

175 h in 1SBF with a pH of 7.2, only a few patches (0.2–0.5 mm^2 in area) of apatite films were seen here and there on Si (1 0 0) substrate. This severe orientation dependence suggests that the interface energy between the substrate and apatite was an important factor in controlling nucleation [47] of apatite in the simulated physiological solution.

Fig. 2 shows how the thickness of apatite films on Si (1 1 1) increased with deposition time in 1SBF, 2SBF and 2SBF with flushing every 24 h. Each solution was maintained at a pH of 7.2, and the gap between the AW-glass plate and the substrate was always 0.7 mm. In every case the growth rate of the films was low in the first 48 h, but the thickness increased rapidly during the next 72 h, eventually reaching plateaus. In 336 h the thickness of the film in 1SBF was 7.1 μm, while that in 2SBF was 12.7 μm. This larger thickness in 2SBF (having ion concentrations twice those in 1SBF) indicates that supersaturation of the solution in the gap between the AW-glass plate and the substrate played an important role in the deposition of apatite films. This will be discussed further in a future section on the mechanism of deposition. With increasing time the concentration of ions in the solution decreased owing to deposition of apatite film on the substrate and on the walls of the container. When 2SBF solution was flushed every 24 h with fresh solution, the thickness of the apatite film on Si (1 1 1) reached a higher value of 16.2 μm in 336 h (Fig. 2). Many films used in the present study were grown in 2SBF with flushing every 24 h. However, even after flushing with the new solution, there was a plateau in the thickness of the film, due to exhaustion of the dissolvable phase in the AW-glass plate, such that the glass could no longer supply ions to cause supersaturation in the gap between the glass plate and the substrate. In the next section we identify the dissolvable phase in AW-glass.

Another interesting point is that the sluggish growth of the films at the beginning of deposition (first 48 h) may be due to an incubation time needed for nucleation of apatite. This explanation is corroborated by our observation that, when the solution was agitated by a magnetic stirrer rotating at 60 rpm, there was hardly any film growth on Si (1 1 1) in 175 h. Because of the stirring the locally supersaturated solution could not stay in contact with the substrate for long enough to cause appreciable nucleation of the apatite.

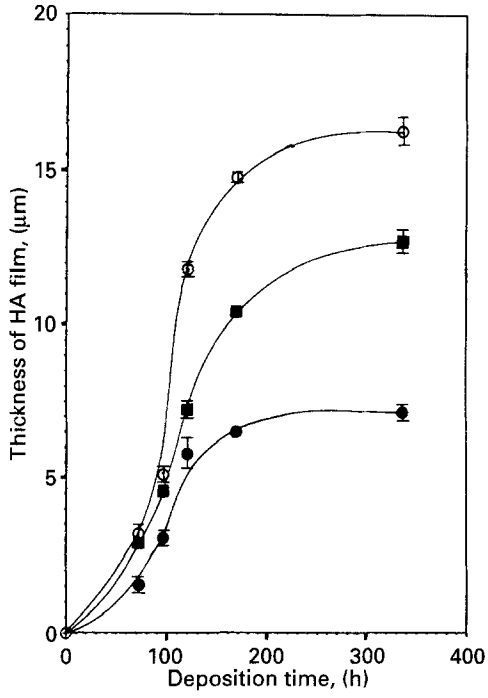

Figure 2 Thickness of films on Si (1 1 1) against the deposition time: (●) 1SBF; (■) 2SBF; and (○) 2SBF with flushing every 24 h, respectively. The pH of each solution was maintained at 7.2.

3.2. X-ray diffraction

Fig. 3a shows the powder X-ray diffraction pattern of AW-glass prepared by sintering at 1300 °C for 2 h in air. The high background noise in the pattern was produced by amorphous calcium phosphate. The pattern also contained the peaks of HA, α-wollastonite ($CaSiO_3$) and β-tricalcium phosphate (TCP). Crystalline phases were formed because we prepared AW-glass by partial melting and slow cooling. Amorphous calcium phosphate, being a metastable phase with a free energy higher than those of its crystalline counterparts, leached into the simulated body fluid, leaving the crystalline phases in the glass plate. Fig. 3b, c shows the X-ray diffraction patterns of the powder scraped from the upper surface (about 0.25 mm thick layer) of the plate of AW-glass after dipping into a 1000 ml solution of 1SBF (with pH of 7.2) at 36 °C for 168 and 336 h, respectively. With increasing time of immersion, the background noise in the patterns decreased and the intensities of the peaks corresponding to the crystalline phases increased. After 336 h of immersion the background intensity (Fig. 3c) at $2\theta = 18°$ was almost the same as that at $2\theta = 52°$, indicating that almost all of amorphous calcium phosphate had leached out.

Fig. 4a–c shows the powder X-ray diffraction pattern of the films scraped from the Si (1 1 1) surface after immersion for 168 h in 2SBF maintained at pH values of 7.2, 8.4 and 9.2, respectively. The films grown at all three values of pH contained a large amount of amorphous calcium phosphate, as indicated by large background noise in the diffraction patterns. The film

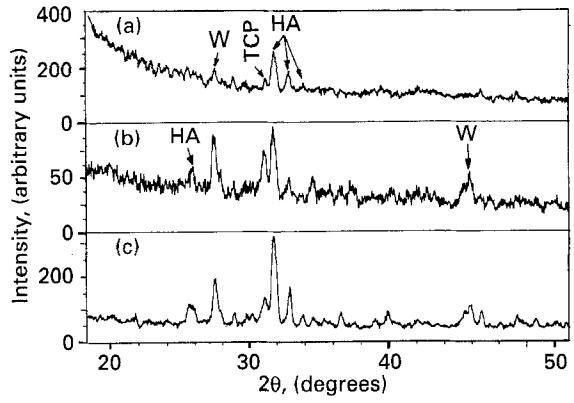

Figure 3 Powder X-ray diffraction patterns of AW-glass: (a) in as-prepared condition; (b) after dipping for 168 h in 1SBF with pH of 7.2 at 36 °C; (c) after dipping for 336 h in 1SBF with pH of 7.2 at 36 °C. W, TCP and HA denote α-wollastonite, β-tricalcium phosphate and hydroxyapatite, respectively.

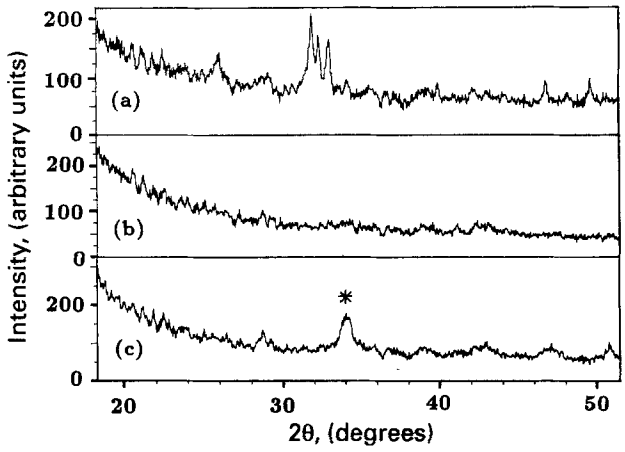

Figure 5 Powder X-ray diffraction patterns of films upon annealing at 800 °C for 3 h in argon. The films were grown for 168 h in 2SBF maintained at various pH values: (a) pH = 7.2; (b) pH = 8.4; (c) pH = 9.2. *, unidentified peak.

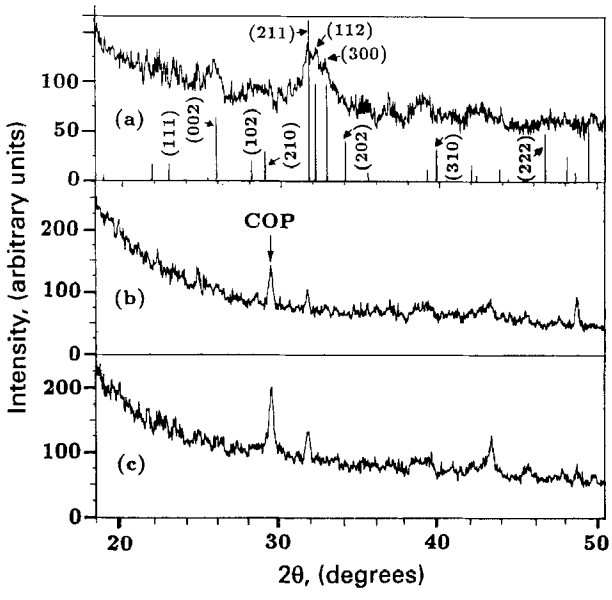

Figure 4 Powder X-ray diffraction patterns for films grown on Si (1 1 1) for 168 h in 2SBF maintained at various pH values: (a) pH = 7.2; (b) pH = 8.4; (c) pH = 9.2. COP stands for calcium oxide phosphate.

grown at pH of 7.2 contained HA and β-TCP. The vertical lines in Fig. 4a indicate the theoretical peaks of HA with the length of line representing the intensity. At higher values of pH (8.4 and 9.2) the intensities of HA peaks decreased, instead a peak near $2\theta = 29°$ developed due to formation of calcium oxide phosphate ($Ca_4O(PO)_2$). Fig. 5a–c shows the powder X-ray diffraction patterns of the films grown at pH values of 7.2, 8.4 and 9.2, respectively, upon annealing at 800 °C for 3 h in argon. HA peaks in the annealed film grown at a pH of 7.2 increased in intensity and became sharper (Fig. 5a). However, the annealing decomposed HA in the films grown at pH values of 8.4 and 9.2, leaving films composed almost entirely of amorphous calcium phosphate (Fig. 5b, c). As will be shown in the next section, HA phase present in the films grown at pH values of 8.4 and 9.2 was highly defective with Ca/P ratios widely different from 1.67. Such defective HA decomposed [30] during the annealing treatment.

Fig. 6a, b shows the X-ray diffraction patterns (in the reflection mode) of the films grown in 2SBF (pH 7.2) on Si (1 1 1) for 168 h in the as-deposited condition and after annealing at 800 °C for 3 h in argon, respectively. The diffraction patterns exhibited strong texture, as the film grew mostly along the [1 0 2] orientation of the HA crystal. In the powder diffraction pattern of pure HA the intensities of the (1 0 2) and (2 1 0) peaks are only 12% and 18%, respectively, of the intensity of (2 1 1), the strongest peak (Fig. 4a). For as-grown films on Si (1 1 1) the intensities of (1 0 2) and (2 1 0) peaks were 4.0 and 1.3 times, respectively, the intensity of (2 1 1) peak (Fig. 6a). Upon annealing the films at 800 °C for 3 h in argon, the background noise in the diffraction pattern (Fig. 6b) decreased owing to crystallization of amorphous calcium phosphate, and the intensities of (1 0 2) and (2 1 0) peaks were 8.1 and 6.4 times, respectively, the intensity of (2 1 1) peak. Thus, (1 0 2) and (2 1 0) peaks in the annealed films were much more intense than the corresponding peaks in the as-grown films. This increase in the proportions of the crystallites with (1 0 2) and (2 1 0) texture might be due to two processes: first, during annealing many HA crystallites rotated and aligned their [1 0 2] and [2 1 0] orientations along the growth direction; secondly, the crystallization of amorphous calcium phosphate involved solid-phase epitaxy [48] and proceeded along preferred orientations.

3.3. Ca/P ratio

Fig. 7 shows the Ca/P ratio against pH for films in the as-grown condition and after annealing at 800 °C for 3 h in argon. The films were grown in 2SBF on Si (1 1 1) for 168 h. Below a pH of 7.5 the as-grown films were Ca-deficient, but above a pH of 7.5 the Ca/P ratio increased rapidly, reaching a value of 4.15 at a pH of 9.2. The high values of the Ca/P ratio beyond a pH of 8.4 indicated that HA was replaced by other phases (see Section 3.2), even though hydroxyapatite is known [49] to be the most stable (least soluble) of all calcium phosphate phases in alkaline pH. It should also be noted that high pH values (> 8.0) obstructed

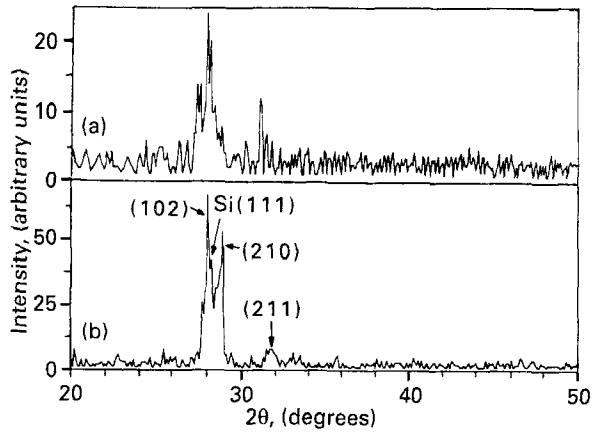

Figure 6 X-ray diffraction patterns (in reflection mode) of films grown for 168 h on Si (1 1 1) in 2SBF maintained at pH of 7.2: (a) as-grown film; (b) after annealing at 800 °C for 3 h in argon.

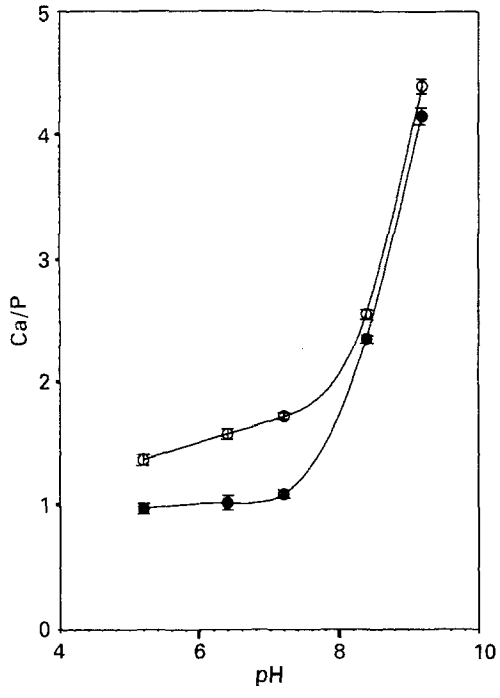

Figure 7 Ca/P ratio of films grown in 2SBF against pH: (●) as-grown; and (○) annealed. The annealing was at 800 °C for 3 h in argon.

deposition of the film. Upon deposition for 336 h in 2SBF with pH values of 8.4 and 9.2, patches of films covered Si (1 1 1) only partially.

The Ca/P ratio of the annealed films against pH showed a similar behaviour (Fig. 7) to that of the unannealed films, but the Ca/P values for the annealed film were higher than those for the unannealed film at the corresponding pH levels. For example, at pH of 7.2 (prevailing in physiological conditions) the Ca/P ratios of the films before and after annealing were 1.10 and 1.72, respectively. Thus, annealed films grown at pH of 7.2 contained HA of high quality. Furthermore, as we will discuss in Section 3.5, annealing improved adhesion between the film and the substrate. Consequently, apatite films, grown in simulated body fluids at a pH of 7.2 and subsequently annealed, have potential for use as coating on biological implants.

3.4. Microstructure and morphology

Fig. 8a is an optical micrograph of an AW-glass plate in the as-sintered condition, showing the porosity. Fig. 8b, c shows optical micrographs of the AW-glass plate after dipping the couple consisting of the plates of glass and Si into 1SBF maintained at pH of 7.2 and 36 °C for 168 and 336 h, respectively. All the micrographs were taken after grinding off a 0.5-mm-thick layer from the top surface of the AW-glass plate and

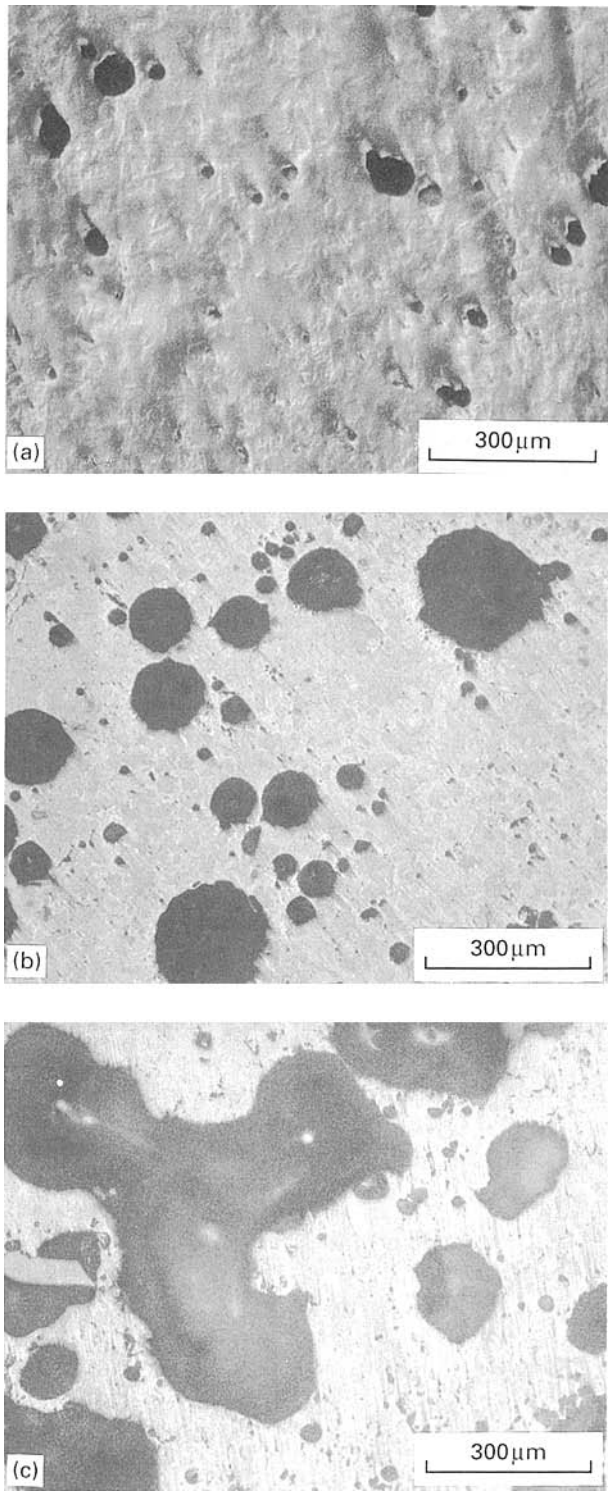

Figure 8 Optical mircrographs of AW-glass plate showing the increase in porosity due to leaching: (a) as-prepared glass; (b) after dipping in 1SBF at pH of 7.2 for 168 h; (c) after dipping in 1SBF at pH of 7.2 for 336 h.

then polishing metalographically. The average size of pores in the as-sintered plate is about 50 μm. Upon immersion into 1SBF the pore size in the glass plate increased owing to leaching of amorphous calcium phosphate. The average pore sizes after dipping into 1SBF for 168 and 336 h were approximately 100 and 200 μm, respectively. In the plate dipped for 336 h, many pores became interconnected, creating holes of size as large as 1 mm (Fig. 8c) and passing through the whole thickness of the glass plate. Thus, in 336 h, leaching took place from the whole plate (5 mm thick) through the interconnected pores.

Fig. 9a–c show the optical micrographs of the surface of the films grown in 2SBF at pH of 7.2 for 72, 168

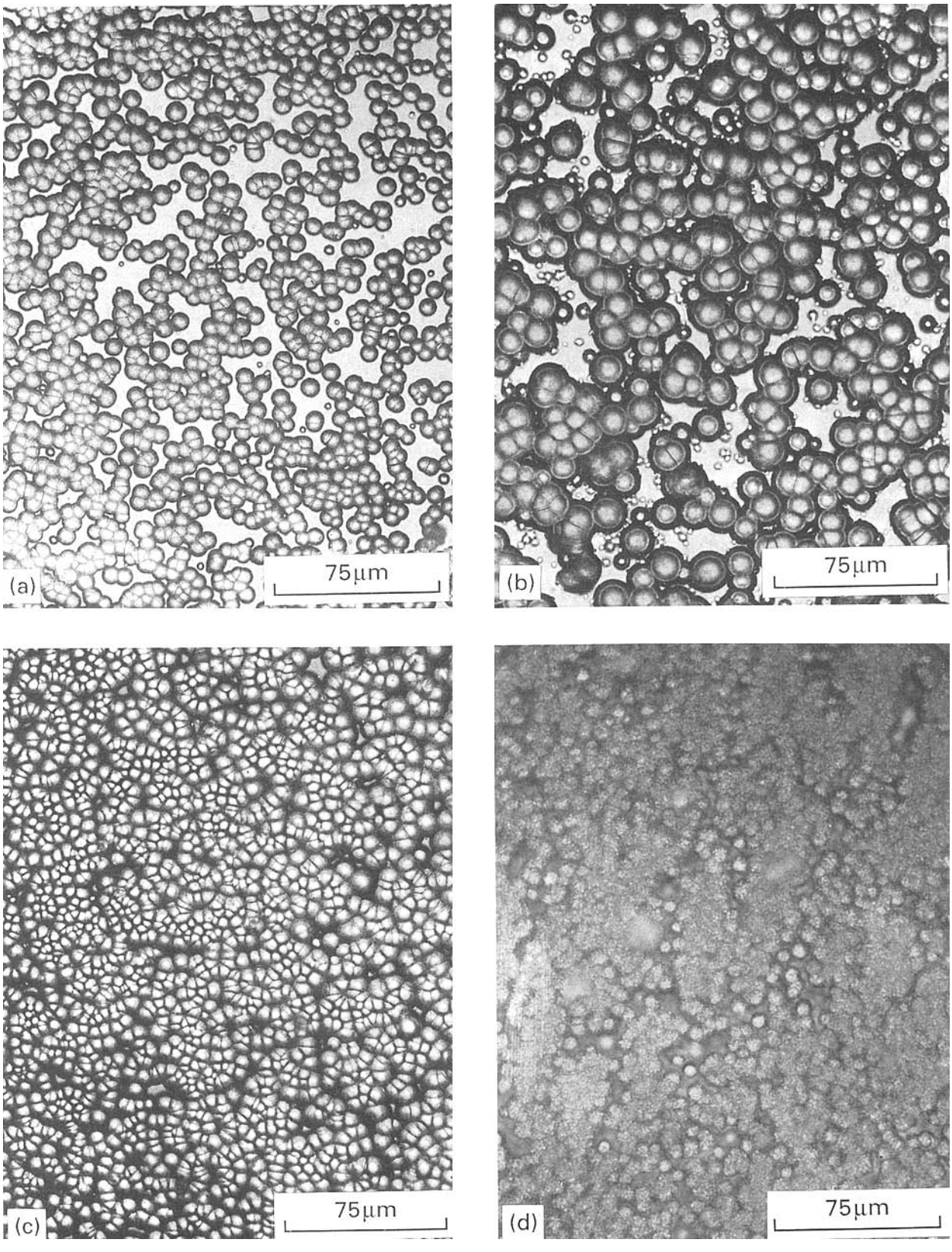

Figure 9 Optical micographs showing growth of apatite islands on Si (1 1 1) in 2SBF at pH of 7.2: (a) after 72 h of dipping; (b) after 168 h; (c) after 336 h; (d) after 336 h of dipping and subsequently annealed at 800 °C for 3 h in argon.

and 336 h, respectively. Spherical islands of calcium phosphate nucleated on Si (1 1 1), grew in size with increasing immersion time and eventually impinged one another. In 336 h the islands were in contact with one another, covering the whole substrate (Fig. 9c). Fig. 9d shows the optical micrograph of the film grown for 336 h in 2SBF and subsequently annealed at 800 °C for 3 h in argon. Due to diffusion during the annealing the surface of the film became smoother. Closer examinations with the help of SEM still showed the hillocks in the annealed films. Fig. 10a, b shows the scanning electron micrographs of the cross-section of the films, grown in 2SBF at pH of 7.2 for 168 and 336 h, respectively; the films were subsequently annealed at 800 °C for 3 h in argon. The annealed film was sectioned in the middle part by breaking the Si substrate. The electron beam in SEM hit the cross-section at an angle of about 45°. In films grown for 168 h the spherical cap-like islands were seen (Fig. 10a). In films grown for 336 h the islands merged together (Fig. 10b), but still the surface of the film was wavy with the remnants of the hillocks. Each island contained many fibre-like crystallites (Fig. 10b) elongated along the normal to the substrate. These crystallites presumably produced texture in the film (Fig. 6b).

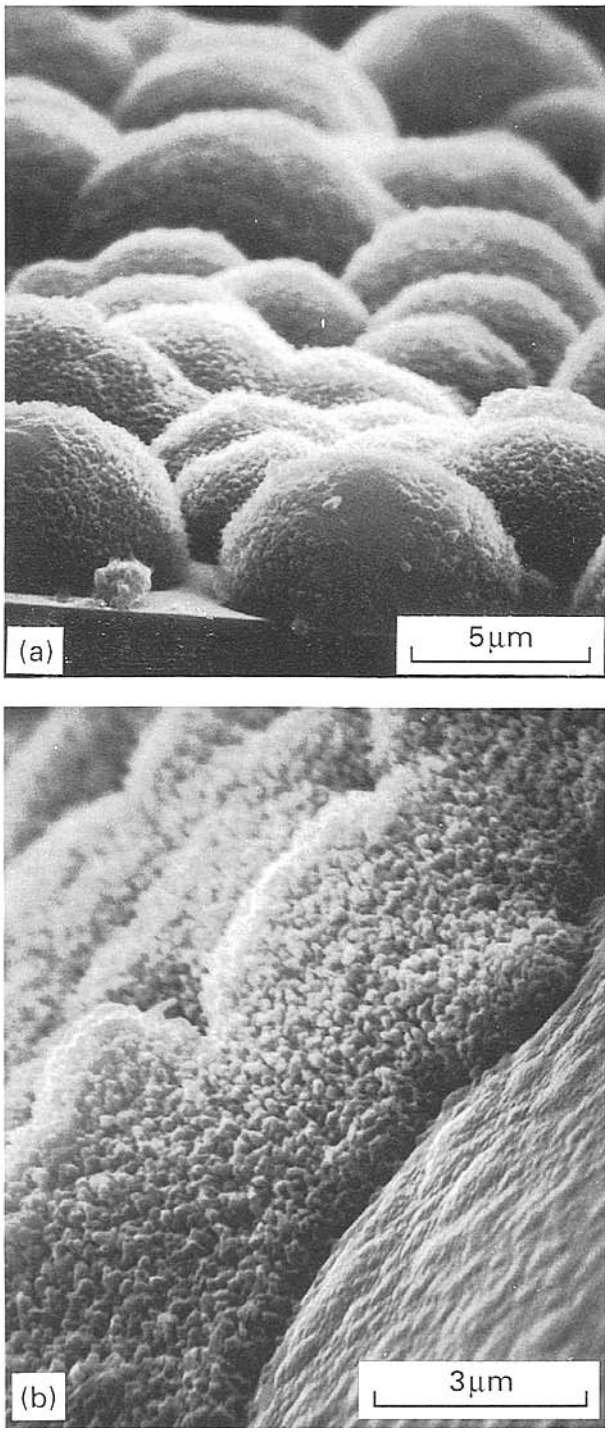

Figure 10 Scanning electron micrographs of apatite films grown in 2SBF at pH of 7.2 and subsequently annealed at 800 °C for 3 h in argon: (a) grown for 168 h; (b) grown for 336 h.

3.5. Microhardness and adhesion

Fig. 11 shows the impression of Vickers indentation on as-grown film under a load of 100 g. The film was deposited on Si (1 1 1) in 2SBF at pH of 7.2 for 336 h. The load was high enough to generate cracks in the corners of the impression. In Fig. 11 the surface of the film was in the focus of the optical microscope. During measurement of the diagonal length of the impression, focusing was done on the impression. Fig. 12 shows plots of the diagonal length of the impression against the load on the indenter for as-grown films as well as for films annealed at 800 °C for 3 h in argon. At loads larger than 36 g the lengths of the impressions in both as-grown and annealed films increased rapidly, owing to formation of cracks. The length of impression in the annealed film was always lower than that in the as-grown films at corresponding loads (Fig. 12), showing

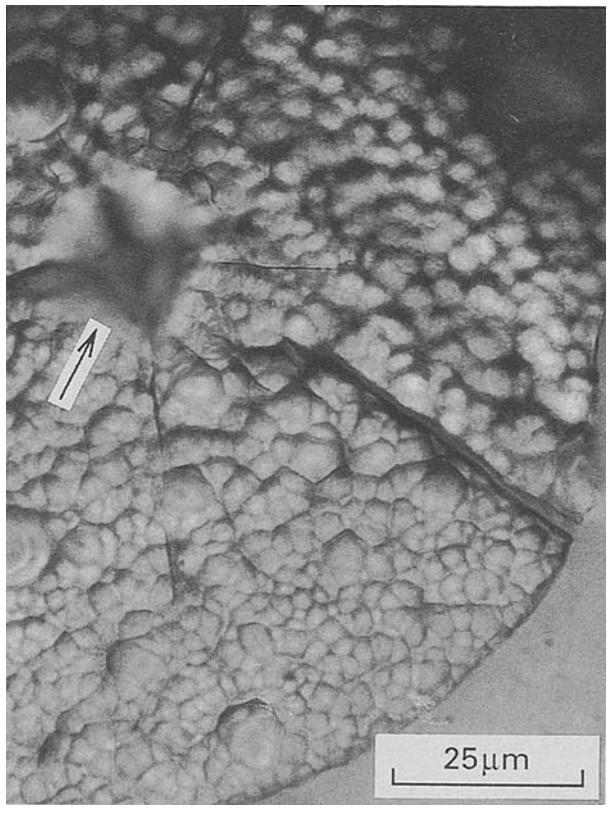

Figure 11 An optical micrograph showing the impression (shown by an arrow) of Vickers indentation under a load of 100 g on an apatite film grown in 2SBF for 336 h.

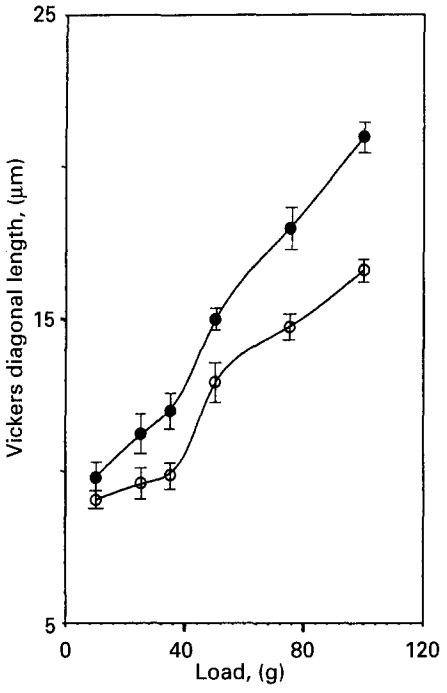

Figure 12 Diagonal length of Vickers impression on apatite films grown in 2SBF for 336 h against the load on the indenter. Films in (●) as-grown condition and (○) after annealing at 800 °C for 3 h in argon.

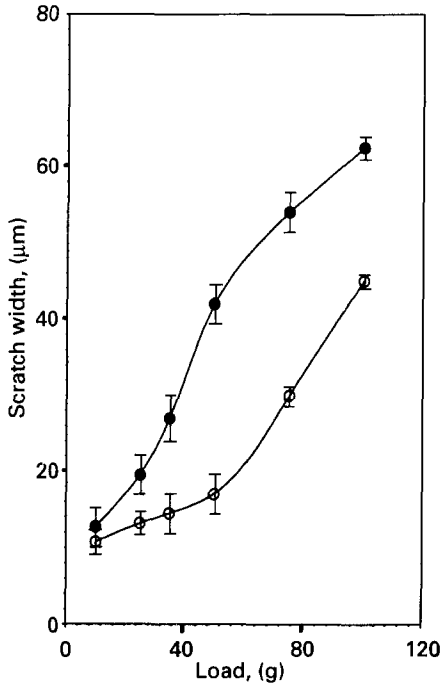

Figure 13 Width of the scratch on apatite films grown in 2SBF for 336 h against the load: (●) as-grown film; and (○) annealed film.

that the annealed films had higher hardness than the as-grown films, possibly due to a sintering effect during the annealing. At a load of 36 g Vickers microhardness of the as-grown and annealed films (as calculated by using Eqn. 1) were 4.5 and 6.7 GPa. It should be noted that Vickers hardness of the underlying Si (1 1 1) surface was 9.3 GPa (measured at 100 g load). The thickness of the film used in indentation tests was 16 μm. At the load of 36 g the tip of Vicker indenter did not touch (as evidenced by the impression length) the Si substrate and thus, hardness of Si did not contribute to the measured hardness of the films.

Fig. 13 shows how the width of the scratch on apatite films grown in 2SBF for 336 h varies with the load for as-grown and annealed films. The scratch widths on the annealed films were always smaller than those on as-grown films at the corresponding loads, indicating that the annealed films were harder. The critical load at which the scratch width increased rapidly due to decohesion of the film was about 50 g for the annealed films; while for as-grown films the scratch width increased rapidly at low loads with the critical load at about 15 g. The adhesion strengths (calculated by using Equation 2) of the as-grown and annealed films were 218 and 639 MPa, respectively. Thus, annealing at 800 °C for 3 h in argon improved significantly the adhesion between the apatite film and Si (1 1 1) substrate. It should be noted that Equation 2 was developed for ductile metal films [45, 46]. Thus, the absolute values of the adhesion strength (calculated by Equation 2) for our apatite films might not be correct, but the comparison of adhesive strengths for various cases still holds true.

3.6. Mechanism

Several authors [35, 37–40] have claimed that hydrated silica is initially formed on the substrate dipped into physiological solution and that this silica induces formation of apatite. Our study, however, showed that apatite film can be grown on a Si (1 1 1) surface and not on a Si (1 0 0) surface, both surfaces being maintained at identical conditions. Thus, formation of a silica layer on the substrate is not a sufficient condition for growth of apatite films. Furthermore, when hydroxyapatite is formed on Si (1 1 1), its crystals grow in a preferred orientation of [1 0 2]. These two facts, namely a lack of growth on Si (1 0 0) and the preferential growth of HA (1 0 2) on Si (1 1 1), indicate that the nucleation [47] of HA crystals depends strongly on the interfacial energy between the nucleus and the substrate. It is worth mentioning that the (1 0 2) plane of HA is rich with oxygen atoms from PO_4 and OH groups [4, 50]. Since Si has a great affinity for oxygen, HA nuclei with the (1 0 2) plane in contact with Si substrate are likely to be formed. Fig. 14a, b shows schematic diagrams of superpositions of oxygen atoms of HA (1 0 2) on (1 0 0) and (1 1 1) planes of Si, respectively. Since Si (1 1 1) is more densely populated than Si (1 0 0), most of the oxygen atoms of HA (1 0 2) are near to Si atoms on Si (1 1 1) and can form strong bonding with them, thereby creating an interface with low energy. This explains the growth of HA crystals with (1 0 2) texture on Si (1 1 1). On the other hand, a higher interface energy between HA (1 0 2) and Si (1 0 0) might preclude formation HA nuclei on Si (1 0 0).

The second important observation of the present study is that local supersaturation near the substrate plays a major role in the growth of apatite film by the solution technique. When the concentrations of ions in the simulated body fluid were made double those in the normal body fluid, the thickness of the film became

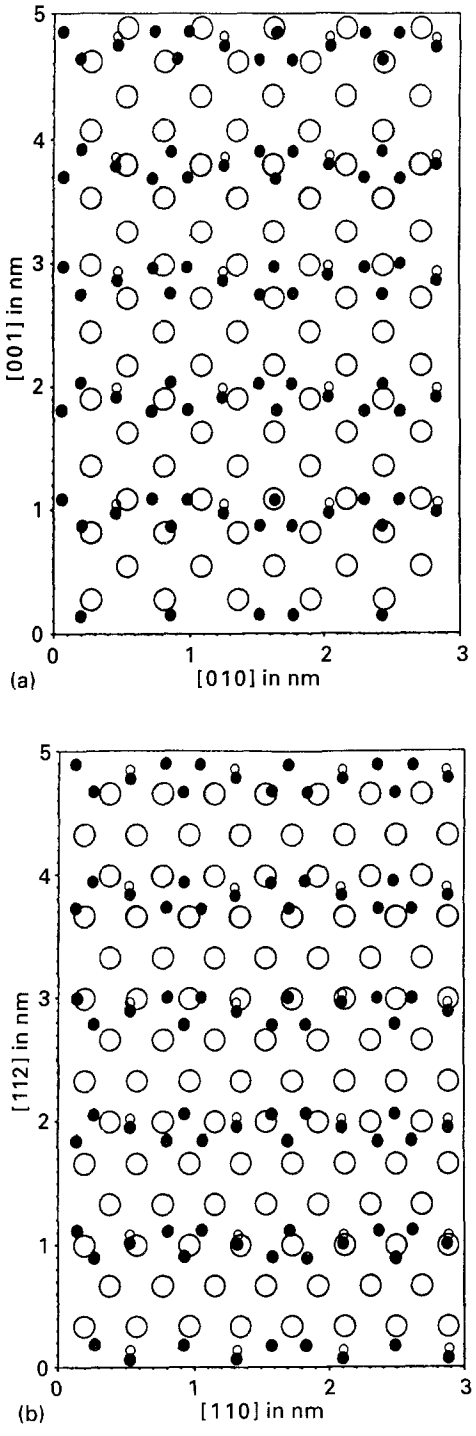

Figure 14 Superposition of oxygen atoms of HA (1 0 2) plane on (a) (1 0 0) and (b) (1 1 1) planes of Si: (○) Si atom in the substrate; (●) oxygen; and (○) hydrogen atoms in HA (1 0 2).

almost double. Leaching of amorphous calcium phosphate from the plate of AW-glass provided supersaturation. When the glass plate became exhausted of amorphous calcium phosphate, the film ceased to grow. We propose that the simulated body fluid becomes locally supersaturated near the substrate and tends to reduce its free energy by depositing atoms on the substrate, thereby growing apatite film. Lowering of free energy (and hence growth of the film) is possible only if the interfacial energy between the substrate and HA nuclei is low. Si does not play any special role in the growth of apatite film, except that Si atoms on the substrate can bond strongly with oxygen atoms in HA nuclei to form interfaces with low energy.

4. Conclusions

Textured films of HA were grown on Si (1 1 1) dipped into a simulated physiological solution. An increase in ion concentrations in the solution increased the film thickness. Leaching of amorphous calcium phosphate from apatite- and wollastonite-containing glass provided supersaturation of the solution. Formation of HA decreased as the pH of the solution was increased above 8.0. Annealing the film at 800 °C for 3 h in argon was beneficial, as it increased the Ca/P ratio, microhardness and adhesion strength of the film. The Ca/P ratio of the film grown in solution at pH of 7.2 and subsequently annealed, was 1.72, which was close to perfect HA. It is suggested that the supersaturated solution reduces its free energy by depositing ions on suitable substrates which can form an interface of low energy with HA.

Acknowledgements

The authors would like to thank professor George Nancollas of the State University of New York at Buffalo for his kind help in the measurement of the Ca/P ratio in HA films.

References

1. C. LAVERNIA and J. M. SCHOENUNG, *Ceram. Bull.* **70** (1991) 95.
2. J. S. HANKER and B. L. GIAMMARA, *Science* **242** (1988) 885.
3. M. JARCHO, *Clin. Orthop. Rel. Res.* **157** (1981) 259.
4. A. S. POSNER, A. PERLOFF and A. D. DIORIO, *Acta Crystallog.* **11** (1958) 308.
5. H. DENISSEN, C. MANGANO and G. VENINI, "Hydroxyapatite implants" (Piccin Nuova Libraria, S.P.A., Padua, 1985) p. 19.
6. R. M. PILLIAR, J. E. DAVIES and D. C. SMITH, *MRS Bull.* **16**(9) (1991) 55.
7. R. E. HOLMES and S. M. ROSER, *Int. J. Oral Maxillofac. Surg.* **16** (1987) 718.
8. J. W. FRAME, P. G. J. ROUT and R. M. BROWNE, *ibid.* **18** (1989) 142.
9. C. CHANG, V. J. MATUKAS and J. E. LEMONS, *ibid.* **41** (1983) 729.
10. G. L. DE LANGE, C. DE PUTTER, K. DE GROOT and E. H. BURGER, *J. Dent. Res.* **68** (1989) 509.
11. S. -Y. CHAO and C. -K. POON, *J. Oral Maxillofac. Surg.* **45** (1987) 359.
12. D. G. PAGE and D. LASKIN, *ibid.* **45** (1987) 356.
13. R. M. PILLIAR and G. C. WEATHERLY, "CRC critical reviews in biocompatibility", Vol. 1 (CRC Press, Boca Raton, Florida, 1986) p. 371.
14. P. E. WANG and T. K. CHAKI, *J. Mater. Sci. Mater. Med.* **4** (1993) 150.
15. J. KOENEMAN, J. LEMONS, P. DUCHEYNE, W. LACEFIELD, F. MAGEE, T. CALAHAN and J. KAY, *J. Appl. Biomater.* **1** (1990) 79.
16. S. R. RADIN and P. DUCHEYNE, *J. Mater. Sci. Mater. Med.* **3** (1992) 33.
17. P. DUCHEYNE, J. BEIGHT, J. CUCKLER, B. EVANS and S. RADIN, *Biomaterials* **11** (1990) 53.
18. P. DUCHEYNE, L. L. HENCH, A. KAGAN, M. MARTENS, A. BURSSENS and J. C. MULIER, *J. Biomed. Mater. Res.* **14** (1980) 225.

19. S. D. COOK, K. A. THOMAS, J. F. KAY and M. JARCHO, *Clin. Orthop. Rel. Res.* **232** (1988) 225.
20. P. DUCHEYNE and J. M. CUCKLER, *ibid.* **276** (1992) 102.
21. P. DUCHEYNE and K. HEALY, *J. Biomed. Mater. Res.* **2** (1998) 1137.
22. P. DUCHEYNE, S. RADIN, M. HEUGHEBAERT and J. C. HEUGHEBAERT, *Biomaterials* **11** (1990) 244.
23. B. L. BARTHELL, T. A. ARCHULETA and R. KOSSOWSKY, Materials Research Society Symposium Proceedings **110** (1989) 709.
24. W. R. LACEFIELD, in "Bioceramics: materials characteristics versus in vitro behavior", edited by P. Ducheyne and J. Lemons (New York Academy of Science, New York, 1988) p. 72.
25. H. HERMAN, *MRS Bull.* **13** (1988) 60.
26. H. OGUCHI, K. ISHIKAWA, S. OJIMA, Y. HIRAYAMA, K. SETO and G. EGUCHI, *Biomaterials* **13** (1992) 471.
27. C. M. COTELL, D. B. CHRISEY, K. S. GRABOWSKI, J. A. SPRAGUE and C. R. GOSSETT, *J. Appl. Biomater.* **3** (1992) 87.
28. H. JI, C. B. PONTON and P. M. MARQUIS, *J. Mater. Sci. Mater. Med.* **3** (1992) 282.
29. M. WEINLAENDER, J. BEUMER III, E. B. KENNEY, P. K. MOY and F. ADAR, *ibid.* **3** (1992) 397.
30. L. G. ELLIES, D. G. A. NELSON and J. D. B. FEATHERSTONE, *Biomaterials* **13** (1992) 313.
31. M. WINTER, P. GRISS, K. DE GROOT, H. TAGAI, G. HEIMKE, H. J. A. V. DIJK and K. SAWAI, *ibid.* **2** (1981) 159.
32. C. P. A. T. KLEIN, A. A. DRIESSEN and K. DE GROOT, *ibid.* **5** (1984) 157.
33. D. F. WILLIAMS, in "Biocompatibility of tissue analogs", Vol. II, edited by D. F. Williams (CRC Press, Boca Raton, Florida, 1985) p. 43.
34. L. L. HENCH, R. J. M. SPLINTER, W. C. ALLEN and T. K. GREENLEE, *J. Biomed. Mater. Res.* **2** (1971) 117.
35. A. E. CLARK, C. G. PANTANO and L. L. HENCH, *J. Amer. Ceram. Soc.* **59** (1976) 37.
36. Y. ABE, T. KOKUBO and T. YAMAMURO, *J. Mater. Sci. Mater. Med.* **1** (1990) 233.
37. L. L. HENCH, *Ann. N.Y. Acad. Sci.* **523** (1988) 54.
38. Ö. H. ANDERSSON, K. H. KARLSSON and K. KANGASNIEMI, *J. Non-Cryst. Solids* **119** (1990) 290.
39. Ö.H. ANDERSSON and K. H. KARLSSON, *ibid.* **129** (1991) 145.
40. T. KOKUBO, *ibid.* **120** (1990) 138.
41. P. LI, Q. YANG, F. ZHANG and T. KOKUBO, *J. Mater. Sci. Mater. Med.* **3** (1992) 452.
42. J. L. GAMBLE, Chemical Anatomy, "Physiology and pathology of extracellular fluid", 6th Edn (Harvard University Press, Cambridge, MA, 1964).
43. A. ISHIZAKA and Y. SHIRAKI, *J. Electrochem. Soc.* **133** (1986) 666.
44. A. GEE and V. R. DEITZ, *Analytical Chem.* **25** (1953) 1320.
45. P. BENJAMIN and C. WEAVER, *Proc. Royal Soc. (London)* **254A** (1960) 163.
46. J. AHN, K. L. MITTAL and R. H. MACQUEEN, in "Adhesion measurement of thin films, thick films and bulk coatings", ASTM STP 640, edited by K. L. Mittal (American Society for Testing and Materials, 1978) p. 134.
47. M. FINE, "Introduction to phase transformation in condensed system (MacMillan, London, 1964).
48. T. K. CHAKI, *Philos. Mag. Lett.* **59** (1989) 223.
49. W. E. BROWN, in "Environmental phosphorous handbook", edited by E. J. Griffith, A. Beeton, J. M. Spencer and P. T. Mitchell (Wiley-Interscience, New York, 1973) p. 203.
50. W. VAN RAEMDONCK, P. DUCHEYNE and P. DE MEESTER, in "Metal and ceramic biomaterials", edited by P. Ducheyne and G. W. Hastings (CRS Press, Boca Raton, Florida, 1984) p. 143.

Received 19 April 1993
and accepted 7 February 1994